IAC-06-C4.P.4.4

MATHEMATICAL MODELING OF HIGH EFFECIENCY PULSED PLASMA THRUSTERS FOR MICROSATELLITES

P. V. Shaw[1] and V. J. Lappas[2]
Surrey Space Centre, United Kingdom
p.shaw@surrey.ac.uk, v.lappas@surrey.ac.uk

ABSTRACT

The Pulsed Plasma Thruster (PPT) is a low cost reliable electric propulsive device that has typical performance within the ranges; specific impulse 300 – 1700 s, Impulse bit 0.06 – 2.6 mN.s and thrust efficiency less than 20%. Past studies have focused on specific aspects to increase performance and understanding, i.e. late time ablation or current sheet canting. Although enlightening, they have yet to increase significantly the efficiency of the PPT. Studies at Surrey Space Centre (SSC) focus on a system design approach to create an efficient PPT. A modified slug parallel plate model published by Worchester Polytechnic Institute, verified with the LES 6, LES 8/9 and Dawgstar PPT data, forms the basis of the SSC optimisation model. The modified model, presented in this paper, works by using a set of coupled differential equations that are solved in MatLab that describe the dynamics of the pulse plasma discharge. Using the SSC optimised model analysis of various thruster parameters leads to the formulation of relationships presented here that describe best-fit curves that can optimise a thruster. This model was used to design a new two stage parallel plate PPT (presented within) which SSC will develop and test, predicting performance within the following ranges; specific impulse 1500 - 5000 s, Impulse bit 0.3 – 0.8 mN.s and thrust efficiency above 60%.

NOMENCLATURE

PPT = Pulsed Plasma Thruster
SSC = Surrey Space Centre
EO = Earth Observing
LES = Lincoln Experimental Satellite
MHD = Magneto Hydrodynamic
PTFE = PolyTetraFluoroEthylene
COTS = Component Of The Shelf
AR = Aspect Ratio
η_t = Thrust efficiency (%)
I_{bit} = Impulse bit (N.s)
m_0 = Mass ablated per discharge (kg)
m = Total mass in current sheet (kg)
E_0 = Capacitor discharge energy (J)
F_{em} = Lorentz force (N)
$F_{initial}$ = Force due to an initial momentum (N)
F_{gas} = Force due to gas dynamic pressure (N)
J = Current density (A m^{-2})
B = Magnetic Field vector (T)
B_{inc} = Self inductance magnetic field vector (T)
h = Distance between electrodes (m)
l = Electrode length (m)
w = Plasma sheet width (m)
δ = Current sheet thickness (m)
A = Area vector (m^2)
x_s = Current sheet trailing edge position (m)
C = Capacitor capacitance (F)
I = Current (A)
V_0 = Initial voltage across capacitor (v)
V_{plasma} = Voltage across plasma (v)
R_{wires} = Wire resistance (Ω)
R_{cap} = Capacitor resistance (Ω)
R_{plasma} = Plasma resistance (Ω)
$R_{electrodes}$ = Electrode resistance (Ω)
R^*_{plasma} = Plasma resistance modified (Ω)
R_{LTA} = Late time ablation resistance (Ω)
L_{wires} = Wire inductance (H)
L_{cap} = Capacitor inductance (H)
$L_{electrodes}$ = Electrode inductance (H)
U_0 = Initial plasma velocity (m s^{-1})
U = Plasma velocity (m s^{-1})
n_e = Debye sphere electron no. density (m^{-3})
n_0 = Average electron number density (m^{-3})
T_e = Electron temperature (K)
K_B = Boltzman Constant (J K^{-1})
σ_{plasma} = Plasma conductivity (Ω m^{-1})
μ_0 = Permeability of free space (Wb A^{-1} m^{-1})
h_p = Planks constant (J.s)
I_e = Ionization energy of Teflon (J)
e, e_i = Charge of an electron/ion (C)
m_e = Electron mass (kg)
ε_0 = Permittivity of a Vacuum (C^2 N^{-1} m^{-2})

1.0 INTRODUCTION

PPT's were first designed and brought to the space propulsion field in the 1960's and gained first flight experience with the Russians on the Zond 2 spacecraft, since then 12 PPTs have flown in space [1]. PPT's offer an attractive alternative to chemical thrusters, argued by Turchi [2], but even with 40 years

[1] Graduate Student, Surrey Space Centre
[2] Assistant Professor, Surrey Space Centre, Member AIAA

of development by university groups and companies PPT's still suffers from poor thrust efficiencies (<20%), where we define thrust efficiency in a PPT as;

$$\eta_t = \frac{I_{bit}^2}{2m_0 E_0} \quad (1)$$

The low thrust efficiencies indicate that a lack in fundamental understanding remains within the field and is highlighted by recent space flight PPT's EO-1 and Dawgstar being designed with thrust efficiencies of 8% and 2.6% respectively [3, 4]. In 1973 The LES 8/9 PPT was designed and meticulously documented, many research groups designed PPT's that copied its performance as a benchmark and applied their theories and research to see how they could build on its performance. Although a lot has been learned on alternative propellant, micro pulsing and plasma plumes [5-11], thrust efficiencies remain low because the community has become focussed on the geometry and design based around the LES 8/9 PPT. SSC develops the work of Laperriere who presented a simple form of MHD coupled differential equations that was verified with the LES 6 and LES 8/9 PPT [12]. The work builds on Laperrieres model and presents theoretical data that suggests potential increases in performance that is achieved by fine-tuning elements of the PPT design. The work additionally presents a new design for a two stage parallel plate PPT that may cut down on late time ablation effects and potentially increases performance.

2.0 PPT FUNDAMENTALS

The PPT is an electric propulsion device that uses the electromagnetic force to accelerate a sheet of neutral plasma, generating thrust in the μN regime. Energy is stored in a high voltage capacitor connected to a pair of parallel plate electrodes. A sparkplug set into the anode discharges an arc, which in analogous comparison with a gas discharge, generates an electron avalanche on the surface of the solid propellant Teflon (PTFE)[13]. The avalanche of electrons creates a closed circuit between the electrodes that allows the capacitor to transfer its energy into the Teflon surface.

This energy is distributed within the surface layers of the Teflon and is used to thermally excite the long fluorocarbon polymer chains, breaking them at random positions at the Carbon – Carbon bonds. Further degradation occurs as the shortened chain fragments 'unzip' to form C_2F_4 monomers.

The thermal excitation is not instantaneous and we can consider the surface of the Teflon in two stages, first is when current passes through it, forming plasma and the second is when the plasma has decoupled from the surface of the Teflon. In the first instance the C_2F_4 monomers are broken up into constituent parts and form neutral plasma of electrons, carbon and fluorine ions. The plasma is accelerated between the electrodes and can be explained by Maxwell's laws of magnetism. As current (J) flows through the neutral plasma it creates a fluctuating electric field. The fluctuations in the electric field produce an induced magnetic field (B). The J x B product generates a Lorentz force in an orthogonal direction, which produces the thrust to propel the satellite.

In the latter instance the C_2F_4 monomers and other longer chain particulates, are not accelerated by any other means other than thermal and pressure expansion. These heavier slower particles exit the thrust chamber over a longer period of time and have a negative effect on the performance of the thruster, this process is known as 'late time ablation'.

PPTs come in two main designs; parallel plate and coaxial design, which describe the main geometry of the discharge electrodes. They can also further be distinguished by the method of feeding the propellant into the discharge gap, whether it is breech fed or side fed. A parallel plate design, shown in Figure 1, maximises on the electromagnetic acceleration, whilst a coaxial design maximises on the electrothermal acceleration, SSC have focussed on designing and optimising the parallel plate breech fed PPT [14].

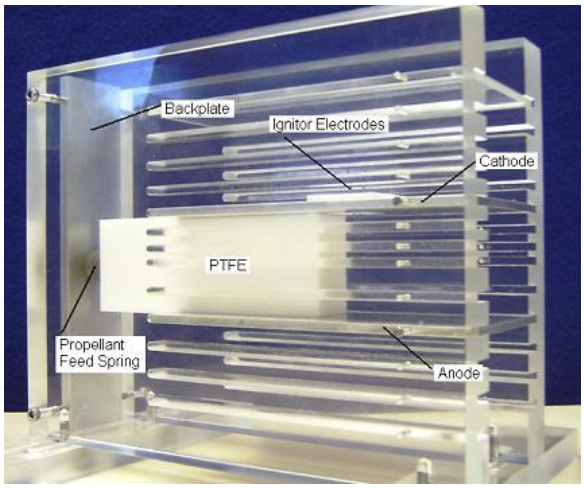

Figure 1. Layout of a Parallel Plate Pulsed Plasma Thruster

2.1 Maximizing Current Density

The parallel plate PPT maximises on electromagnetic acceleration, although there are other effects providing a proportion of the accelerating force, the Lorentz force provides the main bulk of the acceleration. The Lorentz force is derived from Maxwell's laws of magnetism and describes the force on a moving particle when it is subjected to perpendicular magnetic field and flowing current. The Lorentz force is defined as;

$$\vec{F}_{em} = \vec{J} \times \vec{B} \quad (2)$$

There are multiple methods in increasing the accelerating force, by either increasing the magnetic

field or increasing the current density. Increasing the magnetic field was explored by Laperriere and Kimura and was found that although significant increases in impulse bit (~50%) and performance could be made [12, 15], the need for external magnets would increase the mass of the thruster to make it unattainable for space flight.

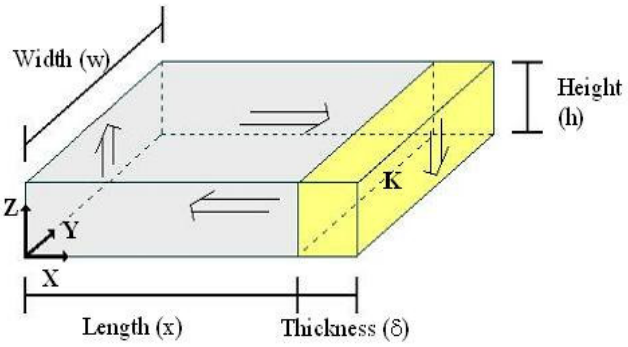

Figure 2. Diagram showing the idealised plasma sheet, the electrodes are situated on the top and bottom of the plasma sheet. The arrows indicate the direction of current flow through the plasma, electrodes and circuitry.

Focussing on increasing the current density J of the plasma sheet is an alternative method in increasing the accelerating Lorentz force. The current sheet is the area of the plasma sheet that has flowing current passing through it at any given time (yellow region in Figure 2). Assuming the current sheet is uniform current density can be defined to be;

$$\vec{J}(t) = -\frac{I(t)}{w\delta}\hat{z} \tag{3}$$

The current in the plasma and current sheet thickness are proven to be very difficult to manipulate, however the plasma sheet width is confined by the discharge chamber width and if sufficient plasma is produced within the discharge chamber then the two are equal. The hypothesis is that by decreasing the width of the plasma sheet by decreasing the chamber width, the current density will be constricted albeit with the same amount of current passing through it. This constriction increases the current density and so increases the accelerating Lorentz force of the PPT.

3.0 MATHEMATICAL MODELLING OF A PPT

The Surrey PPT mathematical model is based on the work of Laperriere on closed control loops for PPTs [12], the work starts by replicating his parallel plate electromechanical model based on a set of coupled differential equations. Once replicated the model was expanded and updated to increase accuracy. Specifics include integrating the impulse bit rather than using a trapezoidal summation, it includes the effects of simple gas dynamic forces and includes a variable resistance model based on current carrying plasmas. The one dimensional parallel plate slug mass model can be considered in three parts, the one dimensional circuit equation, the thrust transfer equation and the plasma resistance model.

3.1 One Dimensional Circuit Equation

Consider the following electrical circuit composing of the following electrical elements, a Capacitor, a pair of parallel plate electrodes and the wires that connect the two in the following circuit.

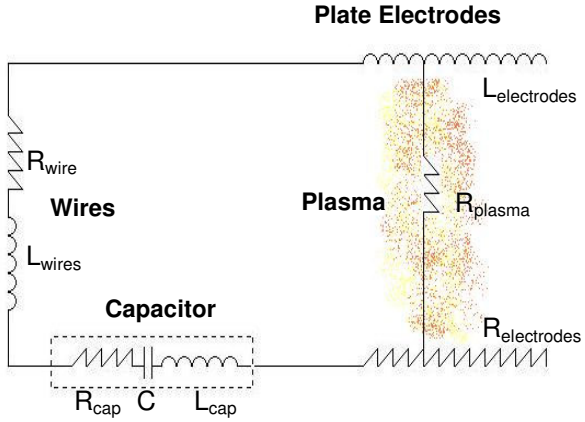

Figure 3. Circuit layout of the PPT

The full derivation of the one dimensional circuit equation is in appendix A and replicates the work presented by Laperriere [12]. It is unclear in the derivation of the boundary conditions used within the plasma sheet in Laperriere work and is expanded upon here, see Figure 2 (the yellow and grey region). To find B_{inc} refer back to the assumption of the ideal one turn solenoid, where it is assumed a uniform current sheet (**K**) i.e. uniform current per unit width) passes through electrodes and wires with infinite conductivity ($\sigma = \infty$) to create a conducting circuit, where the width of the electrodes is much greater than the height.

Assuming infinite conductivity is valid in our theory for the wires and electrodes but in plasma there is a finite conductivity that leads to the current sheet (**K**) having a thickness (δ). Considering the boundary conditions and instigating the Gauss continuity condition B_{inc} of the grey shaded area can be calculated, see Figure 2 [16]. In the normal direction;

$$\nabla \cdot \mu_0 \overline{H} = 0 \rightarrow \oint_s \mu_0 \overline{H} \cdot dA = 0 \tag{4}$$

$$\overline{n} \cdot \frac{B_{inc}}{\mu_0} = 0 \tag{5}$$

In the tangential direction

$$\nabla \times \overline{H} = \vec{j} \rightarrow \oint_s \overline{H} \cdot ds = \int \vec{j} \cdot dA \tag{6}$$

$$\overline{n} \times \frac{B_{inc}}{\mu_0} = K \rightarrow$$

$$B_{inc} = \mu_0 K\hat{y} = \mu_0 \frac{I(t)}{w}\hat{y} \quad (7)$$

The one dimensional circuit equation is thus

$$V_0 - \frac{1}{C}\int_0^t I(t)dt = I(t)\left[R_{cap} + R_{wires} + R_{electrodes} + R_{plasma}\right] + \ldots$$

$$\ldots \frac{dI(t)}{dt}\left(L_{cap} + L_{wires} + \mu_0 \frac{h}{w} x_s(t) + \mu_0 \frac{h}{w}\frac{\delta}{2}\right)\ldots$$

$$\ldots + \frac{dx_s}{dt}\mu_0 \frac{h}{w} I(t) \quad (8)$$

3.2 Thrust Transfer Equation

Newton's second law can explain the physical process of thrust and the mechanisms that contribute to it. Force within the PPT comes from an initial momentum of the fluid, gas dynamics due to build up of pressure within the thruster chamber and a magnetic acceleration from the Lorentz force;

$$\frac{d}{dt}\left[m(t)\frac{dx(t)}{dt}\right] = \sum F_T(t) = F_{initial} + F_{gas} + F_{em} \quad (9)$$

Assuming a neutral charge, single ionization plasma in the model the force equivalent equation becomes;

$$\frac{dm(t)}{dt}\frac{dx(t)}{dt} + m(t)\frac{dx^2(t)}{d^2t} = \frac{d}{dt}mU_0 + \ldots$$

$$\ldots h.w.n_0.k_B.T_e(t) + \int_V (j \times B)dV \quad (10)$$

Solving for the Lorentz force inside the current sheet;

$$\int_V (j \times B)dV = \int_{x_s}^{x_s+\delta}\int_0^w\int_0^h \mu_0 \frac{I(t)}{w}\left[1 - \frac{x - x_s}{\delta}\right]\hat{y} \cdot \ldots$$

$$\ldots\left(-\frac{I(t)}{w\delta}\right)\hat{z}dzdydx \quad (11)$$

$$\int_V (j \times B)dV = \frac{1}{2}\mu_0 \frac{h}{w}\left[I(t)\right]^2 \hat{x} \quad (12)$$

The slug model assumes that once the plasma slug is formed there is no additional mass accumulated to the plasma as it accelerates down the discharge chamber dm(t)/dt = 0, m(t) =m_0. The force equivalent equation becomes;

$$m_0 \frac{dx^2(t)}{d^2t} = \frac{d}{dt}m_0 U_0 + h.w.n_0.k_B.T_e(t)\ldots$$

$$\ldots + \frac{1}{2}\mu_0 \frac{h}{w}\left[I(t)\right]^2 \quad (13)$$

The thrust transfer equation was expanded from Laperriere derivation to include the effects of initial momentum and gas pressure within the discharge chamber [12]. Although a solid propellant PPT is being considered later on the design of a two stage parallel plate PPT is described, where there is a transition between the two pairs of electrodes. The plasma will have a momentum as it enters the second pair of electrodes, so it is important to allow for this effect. However an initial momentum of zero is considered for the standard parallel plate PPT. The gas dynamic force is included to analyse the effects of large density plasma plumes on the overall thrust of the system.

3.3 Plasma Resistance Equation

Solbes presented an equation for the power plasma holds within the discharge chamber working from first principles using Maxwell's equations in the MHD approximation [17];

$$I(t)V_{plasma} = \int_V \frac{j^2}{\sigma_{plasma}}dV + \int_V U \cdot (j \times B)dV \ldots$$

$$\ldots + \int_V j \cdot \frac{\partial A}{\partial t}dV \quad (14)$$

The terms on the right hand side are respectively the joule heating term, the power due to the Lorentz force and an inductive term. The joule heating can be expressed as;

$$\int_V \frac{j^2}{\sigma_{plasma}}dV = \int_{x_s}^{x_s+\delta}\int_0^w\int_0^h \frac{\left[I(t)\right]^2}{w^2\delta^2\sigma_{plasma}}dzdydx \rightarrow \ldots$$

$$\ldots \frac{h \cdot \left[I(t)\right]^2}{w \cdot \delta \cdot \sigma_{plasma}} \quad (15)$$

Converting Equation 15 from power to resistance leaves the expression used by Laperriere in his work. The effects of the power due to the Lorentz force and inductive term are neglected in the SSC model; it is assumed that all the resistance is due to the joule heating term, other wise known as ohmic heating. The resistance of plasma due to ohmic heating is [18];

$$R_{plasma} = \frac{e_i e\sqrt{m_e}\ln\Lambda}{6\pi\sqrt{3}\varepsilon_0^2\left(k_B T_e(t)\right)^{3/2}} \quad (16)$$

Where Lander is known as the plasma parameter and denotes the typical number of particles within the Debye sphere [19];

$$\Lambda = 4\pi n_e \lambda_D^3 \quad (17)$$

Where n_e is the actual number of electrons within the Debye sphere. The Debye Sphere describes the volume of space charge around a point within a plasma that is shielded from the external electric field

with a radius known as the debye length and is expressed as [18];

$$\lambda_D = \left(\frac{\varepsilon_0 k_B T_e(t)}{n_0 e^2} \right)^{1/2} \quad (18)$$

The actual number of electrons (n_e) within the Debye sphere can be approximated from the average number of electrons (n_0) in the plasma with the following relationship.

$$n_e = \frac{4}{3}\pi \lambda_D n_0 \quad (19)$$

Because a quasi-neutral plasma (for every ion there is a single electron) is assumed, we can apply the Saha approximation to predict the average number of electrons in the plasma;

$$n_0 = \frac{1}{h^3}(2\pi m_e k_B T_e(t))^{3/2} e^{\left(\frac{-I_e}{k_B T_e(t)}\right)} \quad (20)$$

Where the Ionisation energy of a Teflon molecule chain is 8.445eV [20]. Assuming that the electron temperature is much greater than the ion temperature and considering the system as a one-turn solenoid $(B = \mu_0 I(t))$ we can derive the electron temperature from the diamagnetic current [18];

$$I_{diamagnetic} = I(t) = (k_B T_e(t)) \frac{B \times \nabla n_0}{B^2} \quad (21)$$

Although several particle drifts occur within current flowing plasma, the most prominent in the PPT consideration, is the diamagnetic drift velocity. The profile of the electron temperature and density calculated in the model are shown in Figure 4, experimental results for electron density on a high thrust PPT is shown in Figure 5 [21]. Comparing the two graphs it is shown that the SSC model is valid up to 20,000 K (10μs), at this point the electron number density decrease in the experimental results, the departure in the SSC model can be explained by the assumptions used in the Saha approximation. The Saha approximation is valid up to a plasma temperature of 20,000 K, where double ionisation then occurs, but as nominal electron temperatures in PPTs are in the range of 40 to 120 thousand Kelvin this suggests that the resistance model is inherently inaccurate [22]. Future work will develop the resistance with a plasma number density equation with a distribution of ions.

The modelled plasma resistance, Figure 6, is compared to the current waveform where it is shown that the resistance remains fairly constant, however when the current in the discharge electrodes reverse there is a large spike in the modelled plasma resistance.

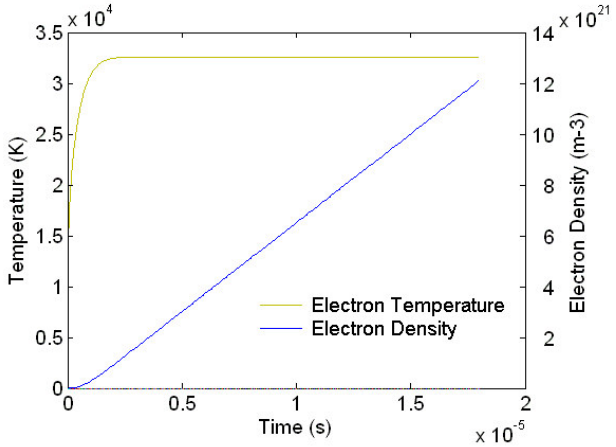

Figure 4. The electron temperature and density profile predicted in the SSC model

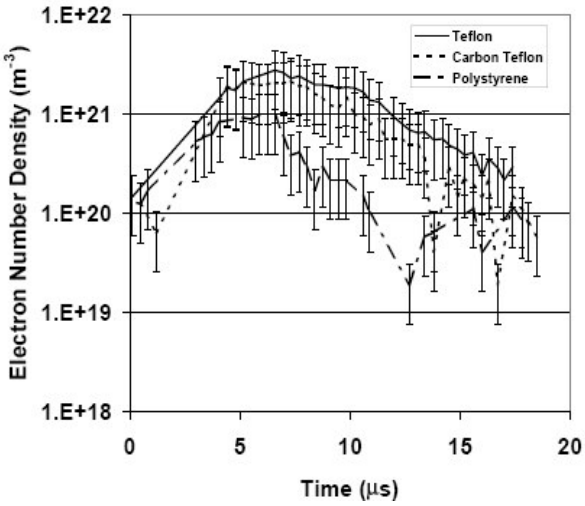

Figure 5. Electron number density data for the NASA High Thrust PPT [21]

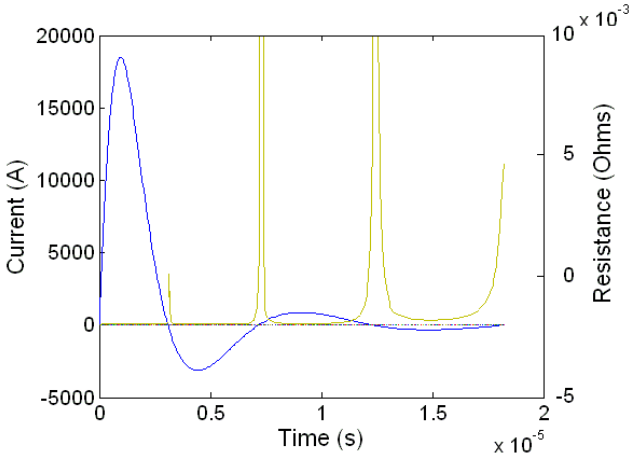

Figure 6. Plasma resistance compared with the current waveform

3.4 Surrey PPT Toolbox

Encoding into MatLab allowed the creation of a Graphical User Interface (GUI) to produce an easy to manipulate toolbox that can model virtual and verify actual PPTs (Figure 7). The user inputs a number of variables either manually or by selecting a well-known PPT like the LES 8/9 thruster. Mission parameters and limits are applied to the model to ensure the most relevant calculations are made, the user if required can focus on the effects of up to three variables simultaneously by applying an iteration protocol. Once the simulation is run the toolbox will display the thruster with the most efficient thrust that it calculated and will allow the user to choose from a number of graphs to study the predicted output of the PPT.

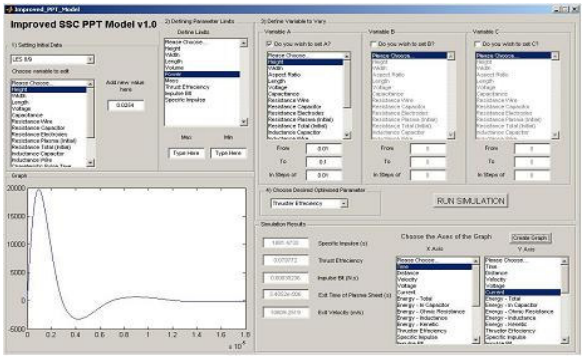

Figure 7. The SSC Toolbox modelling the LES 8/9 thruster

3.5 Late Time Ablation Additional Resistance

The SSC model was run with the LES 8/9 parameters with a circuit resistance of 0.03Ω and an assumed δ = 0.005 m [12], the results of the simulation are shown in Table 1. The model over predicts the actual results by a large margin. Laperriere adjusted and fixed his resistance to match the required output to model the LES 8/9 and LES 6 PPT, arguing and quoting Waltz that the resistance alteration fell within the acceptable uncertainty of the plasma resistance [12, 23].

	Specific Impulse (s)		Impulse Bit (μN.s)		Thruster Efficiency (%)	
	Exp.	Sim.	Exp.	Sim.	Exp.	Sim.
LES-8/9	1000	1200	297	335	6.0	9.8

Table 1. Initial results of the LES 8/9 PPT from the SSC model

SSC modeled a variable plasma resistance and showed that the resistance from the plasma is much less than the required resistance to accurately model the output characteristics of the LES 8/9 thruster. One issue not addressed in Laperrieres work was that of late time ablation, which could be considered as a resistive term slowing the plasma pulse discharge. Considering this as an additional electrical equivalent resistance and factoring into the total resistance we can model the PPT accurately.

$$R_{total} = R_{plasma} + R_{electrodes} + R_{cap} + R_{wires} + R_{LTA} \quad (22)$$

To find the late time ablation resistance the model results are matched to the experimental results, once found it is kept constant through the optimisation process. Table 2 shows the late time ablation equivalent resistances for the PPT's studied with the SSC model.

	R_{LTA} (Ω)
LES 6	0.08
LES 8/9	0.01
Dawgstar	0.15

Table 2. The equivalent late time ablation resistances added to the model to match experimental results.

3.6 Model Verification

The Surrey PPT model was verified with the LES 6, LES 8/9 and Dawgstar PPT parameters; Table 3 shows a comparison between the experimental and simulated results. The addition of the late time ablation resistance allows the model to be set to the experimental results, future work will develop a theory on late time ablation that is dependant on the geometric parameters of the PPT and initial conditions.

	Specific Impulse (s)		Impulse Bit (μN.s)		Thruster Efficiency (%)	
	Exp.	Sim.	Exp.	Sim.	Exp.	Sim.
LES-6	312	312	32	31	3.0	2.5
LES-8/9	1000	998	297	278	6.0	6.8
Dawgstar	266	271	66	67	1.8	1.8

Table 3. A comparison and verification of the SSC model with flight ready PPT's [4, 24]

4.0 SIMULATION RESULTS

4.1 LES 8/9 Investigation

Although there is a need to match the resistances to accurately model the LES 8/9 PPT the SSC model can be used to investigate and develop an understanding about the internal mechanics of the discharge. Table 3 shows the design specifications of the LES 8/9 PPT whilst Table 4 shows its experimental performance capabilities.

Specification of Design	
Discharge Gap Height (Between electrodes)	0.0254m
Discharge Gap Width	0.0254 m
Aspect Ratio (Height/Width)	1
Electrode Length	0.0254 m
Capacitor: Voltage	1538 V
Capacitor: Capacitance	17 μF
Capacitor: Energy Storage	20.1 J
Circuit: Total Inductance	35 nH
Circuit: Total Resistance	0.03 Ω

Table 3. Design specifications of the LES 8/9 PPT [12]

Performance Capabilities	
Specific Impulse	1000 s
Impulse Bit	297 μN.s
Thruster Efficiency	6 %
Exhaust Velocity	9810 m/s
Mass Bit	28.5 μg
Peak Current in Discharge	20 kA

Table 4. Performance capabilities of the LES 8/9 PPT [12]

Early analysis showed that the quantity known as the aspect ratio has a significant role in the optimisation of the PPT. The aspect ratio (AR) can be defined as;

$$AR = \frac{Height(h)}{Width(w)} \tag{23}$$

The quantity of AR can be seen as a multiplication factor in equations 8, 13 and 15. This expresses the importance of this quantity and it's effects on the overall system. A peak is expected where efficiency is optimum because AR will increase the thrust of the system (Eq. 13), whilst increasing the total inductance (Eq 8) and resistance (Eq 15) of the system that negatively affects the performance. For the LES 8/9 PPT we can show that this peak in performance is at an AR of around 10, shown in Figure 8.

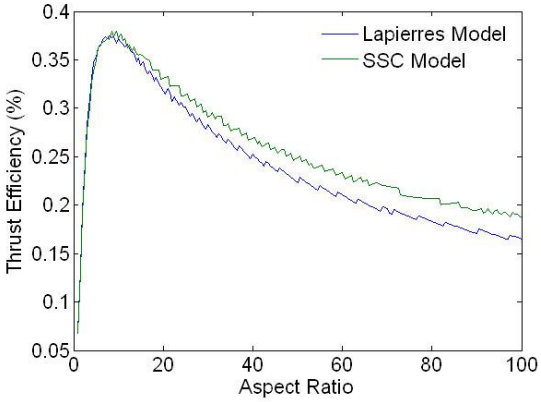

Figure 8. Changing AR for the LES 8/9 thruster

It is important to note the effect of the surface area of the Teflon propellant in the discharge chamber, as some groups believe that increasing the surface area leads to an increase in performance. The model was run for a PPT with the same electrical and discharge characteristics as the LES 8/9 thruster at three different surface areas. The surface areas were kept constant at varying aspect ratios. Figure 9 shows that the surface area of the propellant fuel in relation to the aspect ratio has little effect on the performance of the thruster, i.e. the aspect ratio predominantly defines the performance characteristics of the PPT at any given geometry of the discharge chamber and not the surface area exposed to being discharged.

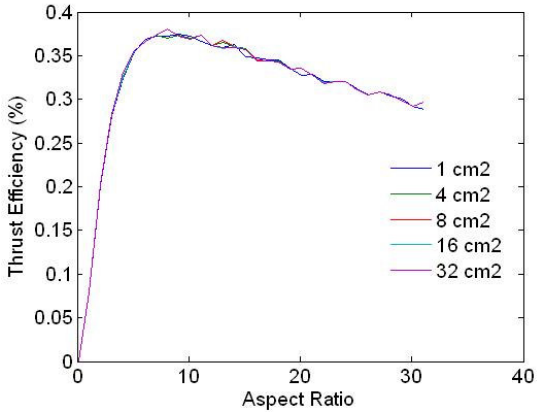

Figure 9. Changing the propellant surface area with AR for the LES 8/9 thruster

The capacitor is a major component of the electrical circuit; the toolbox was programmed to model the geometric and discharge properties of the LES 8/9 PPT allowing for the capacitor properties to be investigated. Figure 10 shows the effect of increasing the capacitance at constant discharge voltage, i.e. the energy was varied in each iteration to maintain a constant voltage. An optimum capacitance at 1538 v is reached at 35μF, which relates to an energy of 42J.

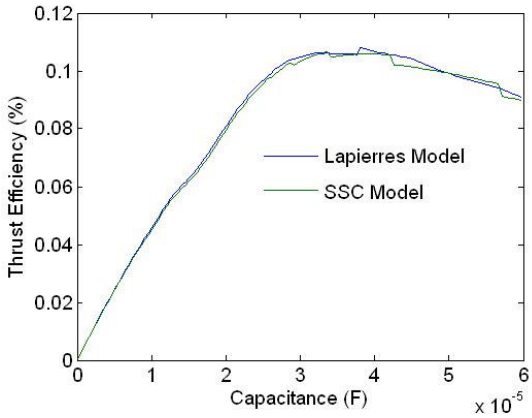

Figure 10. Changing the capacitance of the capacitor for the LES 8/9 thruster

Figure 11 shows the effect of increasing the voltage at constant discharge energy and Figure 12 shows the effect of increasing the discharge energy at constant capacitance, optimum values in each figure are seen at 1100 v and 120 J respectively. In Figures 11 and 12 there are negative spikes where the thrust efficiency tends to zero at specific values and is explained by the resistance spikes seen in Figure 6. The thruster characteristics are measured at the end of the electrodes; if at this time the current reverses there will be a large spike in the plasma resistance that will cause the shown deficiencies in the measured PPT performance.

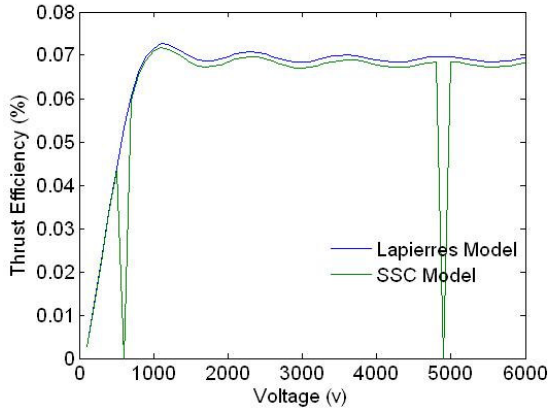

Figure 11. Changing the voltage at constant discharge energy for the LES 8/9 thruster

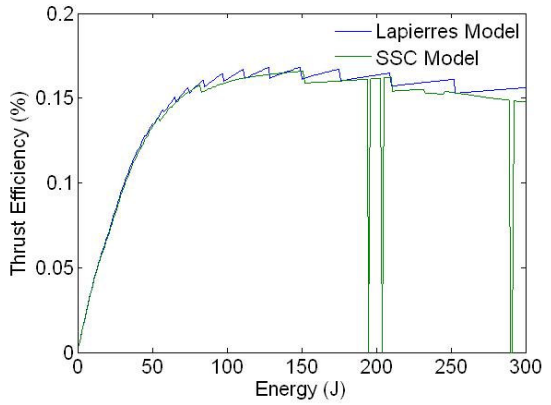

Figure 12. Changing the discharge energy at constant capacitance for the LES 8/9 thruster

Figures 10-12 suggest that for the LES 8/9 thruster there is an optimum capacitor for the specific geometry and discharge properties for that thruster. Investigating further shows that each aspect ratio has a specific optimal capacitor; these were calculated in an iterative program and are shown in Table 5.

AR	E_0 (J)	C (μF)	V_0 (v)	Max Thrust Efficiency. (%)
1	100	11.3	4200	18
4	19	13.0	1700	35
8	7	14.0	1000	42
16	3	12.0	700	52
32	1.2	15.0	400	58

Table 5. Optimum capacitors at specific aspect ratios for the LES 8/9 PPT [12]

Investigating other electrical parameters leads to the conclusion that it is important to keep inductance to a minimum (see Figure 13); Equation 8 indicates methods of how this can be done; tuning the AR, decreasing the current sheet thickness, decreasing the discharge length, decreasing the rate of current change in the discharge pulse or reducing the inductance of the capacitor and electrical wires.

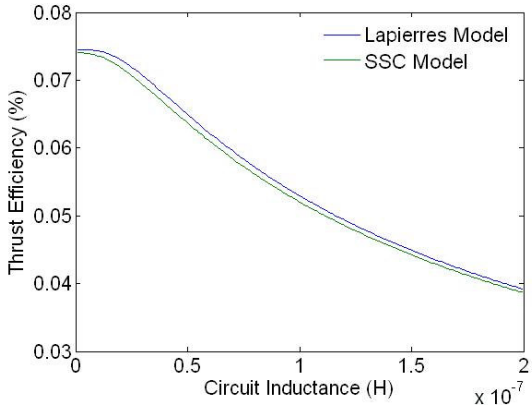

Figure 13. Effects of changing the total inductance for the LES 8/9 thruster

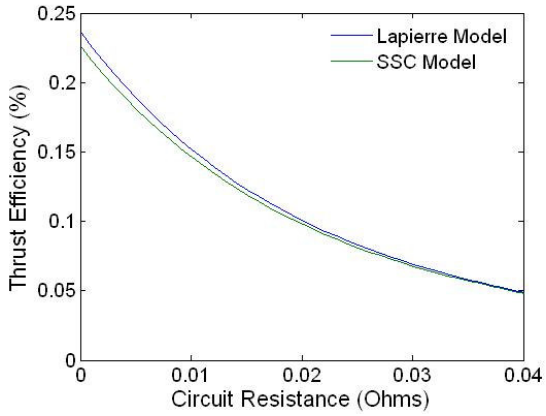

Figure 14. Effects of changing the total resistance for the LES 8/9 thruster

Resistance in the model accounts for significant losses within the LES 8/9 PPT. Figure 14 shows that by decreasing the total resistance in the circuit there is an exponential like increase in performance. Equations 8, 15 and 22 indicate reasonable methods of reducing the total resistance. Minimising resistance in the wires, capacitor and electrodes can be achieved by careful selection of COTS components, whilst novel geometries may decrease the effect of late time ablation. Equations 16 – 21 indicate that plasma with high electron temperature and low average electron density will decrease the plasma resistance.

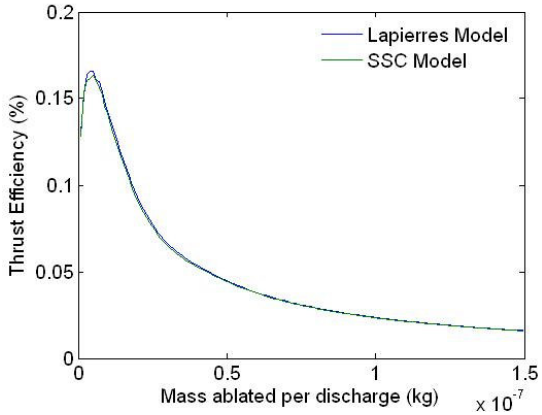

Figure 15. Changing mass bit for the LES 8/9 thruster

The mass bit, which is the amount of propellant ablated per discharge, is difficult to manipulate without using alternative gas or liquid fuels with complex feed mechanisms [5]. In solid fuel PPT's the mass bit will vary from shot to shot, the effects of the mass bit on the thruster efficiency for the LES 8/9 PPT is shown in Figure 15 and shows an optimum mass bit at 10µg. The LES 8/9 PPT capacitor was used to compare varying mass bits at a range of aspect ratios and how this affected the overall system, Figure 16.

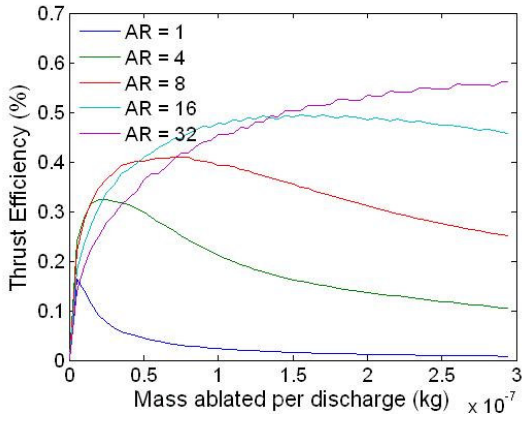

Figure 16. Changing mass bit at various aspect ratios for the LES 8/9 thruster

The plot shows that as the aspect ratio is increased the mass bit required to reach optimum thrust efficiency increases. Also at higher aspect ratios the spread in mass bit has less effect on the performance of the thruster.

4.2 Summary

This investigation has shown that reducing the width with respect to the height of the discharge chamber, (otherwise increasing the aspect ratio), beneficially affects the performance of the PPT in various areas. With respect to the LES 8/9 thruster a maximum of 36% thruster efficiency could have been achieved if the geometry was changed to an AR of around 10. Further optimisation could have been achieved if an optimal capacitor was used or if a reduction in circuit inductance and resistance could have been made. Additionally use of high aspect ratio designs reduce the effects of shot to shot variations in performance characteristics.

5.0 SURREY PPT DESIGN

Investigations have shown that advancements in the PPT are achievable and although the models lack in experimental results it does point in the direction of solid research to be undertaken.

The SSC PPT model makes several assumptions the most significant being the late time ablation resistance and how it remains constant as various parameters of the thruster are optimised. In practice the late time ablation term will vary significantly hence the need to minimise the effect of late time ablation before the plasma is accelerated.

Late time ablation is produced when heating effects in the Teflon surface cause it to ablate after the plasma has decoupled with the surface, these particulates cause detrimental effects to the performance of the thruster. SSC has decided to tackle this problem by once again considering the effects of current density. SSC suspects that if current density can be delivered at low levels this will decrease the heating of the Teflon surface but still be enough to form the plasma, this will theoretically keep late time ablation to a minimum. The current density however needs to be very high to give an optimum discharge. These two effects are at ends with each other and to find equilibrium between the two significantly deteriorates the performance of a standard parallel plate PPT design.

SSC has decided to focus on a new design of PPT that can be thought of as using two sets of parallel plate electrodes set perpendicular to each other. In reality it is one electrode but the physics that apply in the two parts of the electrode have different effects on the plasma within the discharge chamber. Figure 17 shows the basic design of the thruster whilst Figure 18 explains the method of discharge. The first set of electrodes in the plasma forming area run parallel with the Teflon propellant; these long electrodes are designed to deliver the initial energy of the capacitor at a low current density with a significant large width and low AR. This will hopefully keep surface temperature levels to a level that does not create large late time ablation effects. Once the plasma forms and decouples from the surface of the Teflon the electrical energy delivered by the capacitor has no choice but to flow through the side electrodes that are designed to be in optimised configuration, with a high aspect ratio.

Analysis of the two-stage PPT design was conducted with Surrey PPT model; Table 6 shows the design and performance capabilities of the modelled two-stage parallel plate PPT.

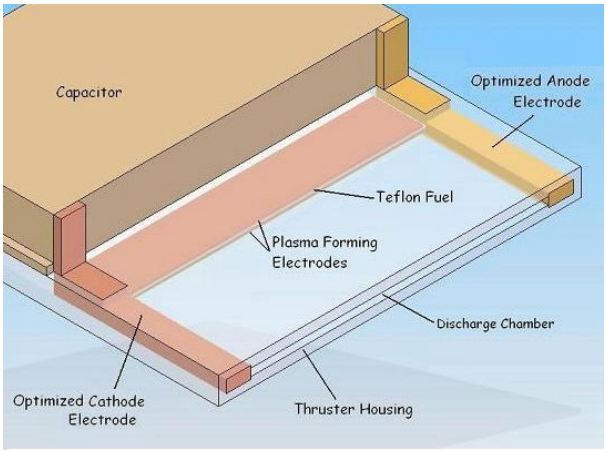

Figure 17. Concept design of Surrey PPT

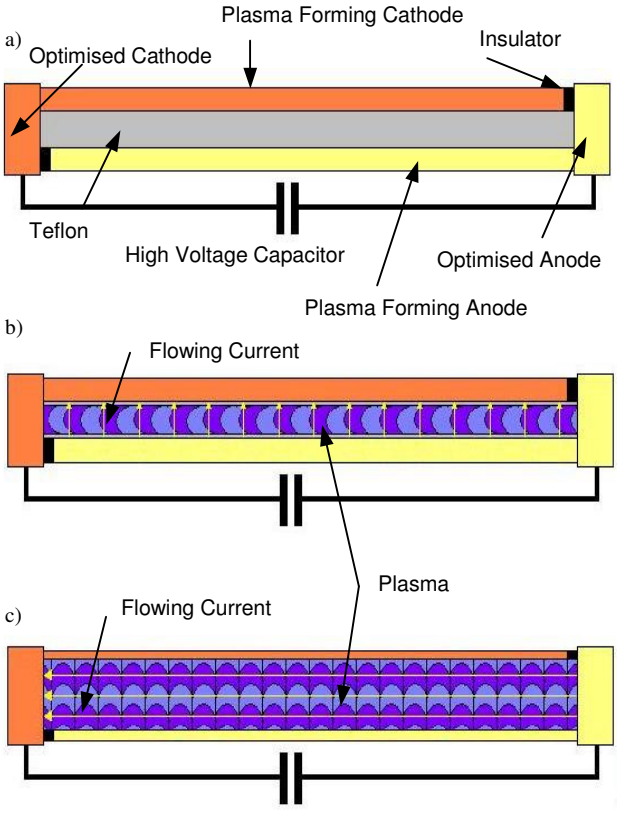

Figure 18. a) View of the PPT looking down discharge chamber. b) Energy builds up in a high voltage capacitor. Once discharge is initiated by a separate sparkplug (not shown), current flows through the Teflon via the 'Plasma Forming electrodes' and creates plasma on the surface of the Teflon.
c) The plasma expands to fill the discharge chamber, the current then flows through the optimised electrodes and plasma creating an overall more efficient discharge.

Two Stage PPT	
Discharge Gap Height (Between electrodes)	0.05m
Discharge Gap Width	0.001 m
Aspect Ratio (Height/Width)	50
Electrode Length	0.05m
Capacitor: Voltage	4200 v
Capacitor: Capacitance	0.89 μF
Capacitor: Energy Storage	7.8J
Circuit: Total Inductance	35 nH
Circuit: Total Resistance	0.013 Ω
Peak Current in Discharge	4 kA
Specific Impulse	4600 s
Impulse Bit	0.3 mN.s
Thruster Efficiency	75 %
Exhaust Velocity	32 km/s
Mass Bit	5.5 μg

Table 6. Design and performance specifications for the two-stage PPT design

Further work will focus on several aspects; The resistance model has to updated in two respects, the first is to account for double and triple ionisation of fluorine and carbon atoms over 20,000 K in the Saha approximation, the second is to develop a late time ablation model based on thruster geometry and conditions during plasma formation. Finally a model for the mass bit has to be added and will also be derived from initial plasma forming conditions.

6.0 CONCLUSIONS

A PPT one dimensional parallel plate model has been developed at SSC that models the performance characteristics of the LES 8/9 PPT accurately. An investigation was undertaken using the SSC model to gain an understanding in the internal mechanics of the parallel plate PPT, the model was applied to the LES 8/9 PPT and showed that simple adjustments to the capacitor and geometric shape of the discharge chamber had significant effects on it's performance. SSC developed on these relationships and presents a new type of two-stage parallel plate pulsed plasma thruster, which focuses on minimizing late time ablation and optimizing on efficient discharge chamber geometries. The SSC model predicts that for a two stage parallel plate PPT it is possible to get performance with; specific impulse of 4600 s, impulse bit of 0.3 mN.s and a thrust efficiency of 75%.

7.0 APPENIX A

7.1 One Dimensional Circuit Equation

The following is the derivation of the one-dimensional circuit equation presented by Laperriere and replicated here to complete this works theory [12].

Start by applying Faradays law around the circuit, shown in Figure 3, within the main text:

$$\oint \vec{E} \cdot ds = -\frac{d\phi_B}{dt} \qquad \text{(A1)}$$

where ϕ_B is the total flux linkage through the circuit. In an ideal solenoid the flux linkage can be described as;

$$\phi_B = \int B.dA = \frac{LI}{N} \quad \text{(A2)}$$

where B is the magnetic field strength, L is the Inductance, I is the current passing through the coils and N is the number of turns within the solenoid. Consider the parallel plate electrodes to be a solenoid of one turn.

$$\oint \vec{E} \cdot ds = -\frac{d}{dt}\left[\phi_{cap}(t) + \phi_{wires}(t) + \phi_{electrodes}(t)\right] \quad \text{(A3)}$$

$$\oint \vec{E} \cdot ds = -\frac{d}{dt}\left[L_{cap} I(t) + L_{wires} I(t) + ... \right.$$
$$\left. ... \iint_{electrodes} B_{inc}(x,y).dA \right] \quad \text{(A4)}$$

The flux linkage can also be described as;

$$\phi_E = \int_i^f \vec{E}.ds = -(V_f - V_i) \quad \text{(A5)}$$

where the subscripts define the initial (i) and final (f) voltages for the system;

$$(V_f - V_i) = \frac{d}{dt}\left[L_{cap} I(t) + L_{wires} I(t) + ... \right.$$
$$\left. ... \iint_{electrodes} B_{inc}(x,y).dA \right] \quad \text{(A6)}$$

Considering Kirchoff's law;

$$\sum V = \sum IR = I(t)\sum R_T = I(t)...$$
$$... \left[R_{cap} + R_{wires} + R_{electrodes} + R_{plasma}\right] \quad \text{(A7)}$$

the initial voltage is then;

$$V_i = I(t)\left[R_{cap} + R_{wires} + R_{electrodes} + R_{plasma}\right] \quad \text{(A8)}$$

The voltage at any given time is then;

$$V_f = I(t)\left[R_{cap} + R_{wires} + R_{electrodes} + R_{plasma}\right] + ...$$
$$... \frac{d}{dt}\left[L_{cap} I(t) + L_{wires} I(t) + \iint_{electrodes} B_{inc}(x,y).dA\right] \quad \text{(A9)}$$

To find B_{inc} refer back to the assumption of the ideal one turn solenoid, where it is assumed a uniform current sheet (**K**) i.e. uniform current per unit width) passes through electrodes and wires with infinite conductivity ($\sigma = \infty$) to create a conducting circuit, where the width of the electrodes is much greater than the height.

Assuming infinite conductivity is valid in our theory for the wires and electrodes but in plasma there is a finite conductivity that leads to the current sheet (**K**) having a thickness (δ). Considering the boundary conditions and instigating the Gauss continuity condition B_{inc} of the grey shaded area can be calculated, see Figure 2 [16]. In the normal direction;

$$\nabla \cdot \mu_0 \overline{H} = 0 \rightarrow \oint_s \mu_0 \overline{H} \cdot dA = 0 \quad (4)$$

$$\overline{n} \cdot \frac{B_{inc}}{\mu_0} = 0 \quad (5)$$

In the tangential direction

$$\nabla \times \overline{H} = \overline{j} \rightarrow \oint_s \overline{H} \cdot ds = \int \overline{j} \cdot dA \quad (6)$$

$$\overline{n} \times \frac{B_{inc}}{\mu_0} = K \rightarrow$$

$$B_{inc} = \mu_0 K \hat{y} = \mu_0 \frac{I(t)}{w} \hat{y} \quad (7)$$

B_{inc} in the yellow region needs to be found, see Figure 2, within the main text, which represents the current sheet. The current density J(t) throughout the sheet is uniform and equal to;

$$J(t) = -\frac{I(t)}{w\delta} \hat{z} \quad \text{(A10)}$$

By considering the boundary conditions between the yellow and grey regions in Figure 2, within the main text, B_{inc} can be found at any position x in the current sheet using the following relationship;

$$\oint_s \overline{B}_{inc} \cdot ds = \mu_0 \int \overline{j} \cdot dA \quad \text{(A11)}$$

$$B_{Yellow} - B_{Grey} = -\mu_0 \int_{x_s}^{x} \frac{I(t)}{w\delta} \hat{z} \cdot dA \quad \text{(A12)}$$

$$B_{inc}(x,t) = \mu_0 \frac{I(t)}{w} \hat{y} - \mu_0 \frac{I(t)}{w\delta}\left[x - x_s\right] \quad \text{(A13)}$$

$$B_{inc}(x,t) = \mu_0 \frac{I(t)}{w}\left[1 - \frac{x - x_s}{\delta}\right]\hat{y} \quad \text{(A14)}$$

A complete description of B_{inc} is given as;

$$B_{inc}(x,t) = \begin{cases} \mu_0 \dfrac{I(t)}{w} \hat{y}, & 0 < x < x_s(t) \\ \mu_0 \dfrac{I(t)}{w}\left[1 - \dfrac{x - x_s}{\delta}\right]\hat{y}, & x_s(t) < x < x_s(t) + \delta \\ 0, & x > x_s(t) + \delta \end{cases} \quad \text{(A15)}$$

Returning to the equation for voltage at any given moment of time and substituting in our value for B_{inc} (x, t);

$$V_f = I(t)\left[R_{cap} + R_{wires} + R_{electrodes} + R_{plasma}\right] + \ldots$$

$$\ldots \frac{d}{dt}\left[L_{cap} I(t) + L_{wires} I(t) + \int_0^{x_s}\int_0^{h} \mu_0 \frac{I(t)}{w} dy dx \ldots \right.$$

$$\left. \ldots + \int_{x_s}^{x_s+\delta}\int_0^{h} \mu_0 \frac{I(t)}{w}\left[1 - \frac{x - x_s}{\delta}\right] dy dx \right] \quad \text{(A16)}$$

Integrating over the electrodes leads to;

$$V_f = I(t)\left[R_{cap} + R_{wires} + R_{electrodes} + R_{plasma}\right] + \ldots$$

$$\ldots + \frac{d}{dt}\left[I(t)\left(L_{cap} + L_{wires} + \mu_0 \frac{h}{w} x_s(t) + \mu_0 \frac{h}{w}\frac{\delta}{2} \right) \right] \quad \text{(A17)}$$

Expanding using the mathematical chain rule and realising that the final voltage is the charging voltage (V_0) the capacitor is charged to minus the voltage discharged in a time (t) by the capacitor, the final equation that describes fully the electrical one dimensional circuit is;

$$V_0 - \frac{1}{C}\int_0^t I(t)dt = I(t)\left[R_{cap} + R_{wires} + R_{electrodes} + R_{plasma}\right] + \ldots$$

$$\ldots \frac{dI(t)}{dt}\left(L_{cap} + L_{wires} + \mu_0 \frac{h}{w} x_s(t) + \mu_0 \frac{h}{w}\frac{\delta}{2} \right) \ldots$$

$$\ldots + \frac{dx_s}{dt} \mu_0 \frac{h}{w} I(t) \quad \text{(8)}$$

8.0 REFERENCES

[1] Hoskins W. A., Rayburn C., "Pulsed Plasma Thruster Electromagnetic Compatibility: History, Theory and Flight Validation on EO-1" AIAA 2003-5016, 39th Joint Propulsion Conference, Huntsville, Alabama, 2003

[2] Burton R. L., Turchi P. J., "Pulsed Plasma Thruster" Journal of Propulsion and Power, Vol. 14, No. 5, 1998

[3] Zakrwski C., Sanneman P., Hunt T., Blackman K., "Design of the EO-1 Pulsed Plasma Thruster Attitude Control Experiment" AIAA-2001-3637, 37th Joint Propulsion Conference, Salt Lake City, Utah, 2001

[4] Rayburn C., Campbell M., "Development of a Micro Pulsed Plasma Thruster for the Dawgstar Nanosatellite" AIAA 2000-3256, 36th Joint Propulsion Conference, Huntsville, Alabama, 2000

[5] Scharlemann C. A., "Investigations of Thrust Mechanisms in a Water Fed Pulsed Plasma Thruster" Dissertation, Department of Aeronautical and Astronautical Engineering, The Ohio State University, 2003

[6] Scharlemann C. A., York T. M., Turchi P. J., "Alternative Propellants for Pulsed Plasma Thrusters" AIAA 2002-4270, 38th Joint Propulsion Conference, Indianapolis, Indiana, 2002

[7] Pencil E. J., Kamhawi H., "Alternate Propellant Evaluation for 100-joule-class Pulsed Plasma Thrusters" AIAA 2003-5171, 39th Joint Propulsion Conference, Huntsville, Alabama, 2003

[8] Arrington L. A., "Evaluation of Pulsed Plasma Thruster Micropulsing" AIAA 2004-3458, NASA/CR-2004-213209

[9] Lin G., Karniadakis G. E., "High-Order Modeling of Micro-Pulsed Plasma Thrusters" AIAA 2002-2872, 3rd Theoretical Fluid Mechanics Meeting, St Louis, Missouri, 2002

[10] Ziemer J. K., Choueiri E. Y., "Scaling laws for electromagnetic pulsed plasma thrusters" Plasma Sources Science and Technology, Vol. 10, pg 395-405, 2001

[11] Keidar M., Boyd I. D., "Device and Plume Model of an Electrothermal Pulsed Plasma Thruster" AIAA 2000-3430, 36th Joint Propulsion Conference, Huntsville, Alabama, 2000

[12] Laperriere D. D., "Electromechanical Modelling and Open-Loop Control of Parallel-Plate Pulsed Plasma Microthrusters with Applied Magnetic Fields" Masters Thesis, Department of Mechanical Engineering, Worcester Polytechnic Institute, 100 Institute Road, Worcester, MA 01609-2280, 2005

[13] Cooley J. E., Choueiri E. Y., "Fundamentals of PPT Discharge Initiation: Undervoltage Breakdown Through Electron Pulse Injection" AIAA 2003-5027, 39th Joint Propulsion Conference, Huntsville, Alabama, 2003

[14] Rysanek F., Burton R. L., "Effects of Geometry and Energy on a Coaxial Teflon Pulsed Plasma Thruster" AIAA 2000-3429, 36th Joint Propulsion Conference, Huntsville, Alabama, 2000

[15] Kimurra I., Yanagi R., Inoue S., "Preliminary Experiments on Pulsed Plasma Thrusters with Applied Magnetic Fields" 13th International Electric Propulsion Conference, San Diego, California, 1978

[16] http://ocw.mit.edu/NR/rdonlyres/Electrical-Engineering-and-Computer-Science/6-641Spring-2005/C6945058-A879-47C6-BF27-2C081E27BAA7/0/lecture1.pdf date evaluated 13/9/06

[17] Solbes A., Vondra R. J., "Performance Study of a solid Fuel-Pulsed Electric Microthruster" Journal of Spacecraft, Vol. 10, No.6, pg 406-41

[18] W. M. Stacey, "Fusion Plasma Analysis", 1st Edition, Krieger, ISBN 0894646028, 1981

[19] Fitzpatrick R., Hazeltine R. D., Waelbroeck F. L., "Introduction to Plasma Physics: A graduate course", University of Texas at Austin, http://farside.ph.utexas.edu/teaching/plasma/lectures/lectures.html date evaluated 18/9/06

[20] Ono M., Yamane H., Fukagawa H., Kera S., Yoshimura D., Morikawa E., Deki K., Ueno N., "Possibility of the Fermi Level Control by VUV-Induced Doping of an Organic Thin Film: Polytetrafluoroethylene" Proc. Int. Symp. Super-Functionality Organic Devices, IPAP Conf. Series 6, pg 27-30

[21] Kamhawi H., Arrington L., Pencil E. J., Haag T., "Performance Evaluation of a High Energy Pulsed Plasma Thruster" AIAA 2005-3695, 41st Joint Propulsion Conference, Tucson, Arizona, 2005
[22] Gatsonis N. A., Zwahlen J., Wheelock A. T., Pencil E. J., Kamhawi H., "Characterization of a Pulsed Plasma Thruster Plume using a Quadruple Langmuir Probe Method" AIAA 2002-4123, 38th Joint Propulsion Conference, Indianapolis, Indiana, 2002
[23] Waltz P.M., "Analysis of a Pulsed Electromagnetic Plasma Thruster" Masters Thesis, Massachusetts Institute of Technology, Department of Electrical Engineering, Cambridge, MA, 1969
[24] Rayburn C., Campbell M., Mattick A.T., "Pulsed Plasma Thruster System for Microsatellites" Journal of Spacecraft, Vol. 42, No. 1,2005